

1 Meta-analysis of permeability literature data shows 2 possibilities and limitations of popular methods

3 Kateřina Storchmannová¹, Martin Balouch^{2,3}, Jakub Juračka^{1,4}, František Štěpánek², and Karel Berka^{1*}

4 ¹ Department of Physical Chemistry, Faculty of Science, Palacký University Olomouc, 17. listopadu 12,
5 771 46 Olomouc, Czech Republic.

6 ² Department of Chemical Engineering, University of Chemistry and Technology, Prague, Technická 3,
7 166 28 Prague 6, Czech Republic.

8 ³ Zentiva k.s., U Kabelovny 130, 102 00 Prague 10, Czech Republic

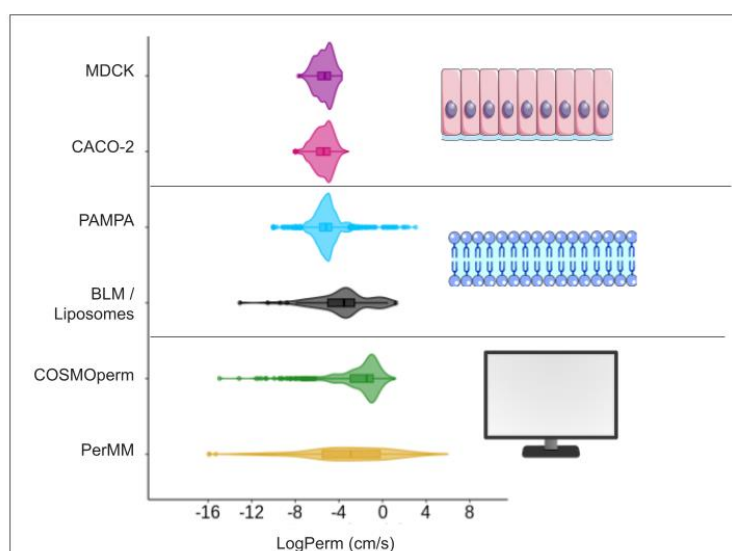
9 ⁴ Department of Computer Science, Faculty of Science, Palacký University Olomouc, 17. listopadu 12,
10 771 46 Olomouc, Czech Republic.

11 * Corresponding author, e-mail: karel.berka@upol.cz

12 Abstract

13 Permeability is an important molecular property in drug discovery, as it co-determines pharmacokinetics
14 whenever a drug crosses the phospholipid bilayer, *e.g.*, into the cell, in the gastrointestinal tract or across
15 the blood-brain barrier. Many methods for the determination of permeability have been developed,
16 including cell line assays, cell-free model systems like PAMPA mimicking, *e.g.*, gastrointestinal
17 epithelia or the skin, as well as the Black lipid membrane (BLM) and sub-micrometer liposomes.
18 Furthermore, many *in silico* approaches have been developed for permeability prediction.

19 Meta-analysis of publicly available databases for permeability data (MolMeDB and ChEMBL) was
20 performed to establish their usability. Firstly, experimental data can only be measured between
21 thresholds for the lowest and highest permeation rate obtainable within physical boundaries. These
22 thresholds vary strongly between methods. Secondly, computed data do not obey these thresholds but,
23 on the other hand, can produce incorrect results. Thirdly, even for the same method and molecule, there
24 is often a strong discrepancy between individual measured values. These differences are based not only
25 on the statistics but also on the varying approaches and evaluation of the measured data. Thus, when
26 working with in-house measured or published permeability data, we recommend to be cautious with
27 their interpretation.



28 Introduction

29 Passive permeability is a critical molecular property studied in drug discovery because of its strong
 30 influence on pharmacokinetics. It plays an essential role in the gastrointestinal absorption of oral drugs,
 31 penetration of the blood-brain barrier (BBB), and renal reabsorption.¹

32 The permeability coefficient ($\text{cm}\cdot\text{s}^{-1}$) is the quantitative measure of permeability, often presented as a
 33 decimal logarithm ($\log\text{Perm}$). Numerous methods for their determination have been developed because
 34 of the importance of permeability coefficients in pharmaceutical research. We can, in general, divide the
 35 approaches into cell-based in vivo experimental assays, membrane-based in vitro experimental essays
 36 and in silico approaches.

37 Among the oldest and best-established methods of permeability measurement are the cell-based colon
 38 carcinoma cell line permeability assay (CACO-2)² and Madin-Darby Canine Kidney cells (MDCK)³.
 39 Permeability measurements are realized in transwell plates. Each well is divided into a donor and an
 40 acceptor compartment, separated by a membrane. In the case of CACO-2 and MDCK, the membrane
 41 consists of a cell monolayer cultured on a solid support. Despite their different origins, the CACO-2 and
 42 MDCK are composed of morphologically analogous cells and are widely used as model intestinal
 43 membranes⁴.

44 Apart from cell-based experiments, there are several in vitro membrane-based methods. The most often
 45 used one is the parallel artificial membrane permeability assay (PAMPA)⁵. The membrane on which
 46 PAMPA methods are based is artificially made and chosen depending on the membrane the assay
 47 mimics. To this date, many variants of PAMPA have been published. The examples include DS-
 48 PAMPA⁶, which mimics gastrointestinal absorption, blood-brain barrier PAMPA⁷, SkinPAMPA⁸, or
 49 nasal-PAMPA⁹. Another long-time-known experimental method of permeability measurement is BLM
 50 (Black Lipid membrane), first published by Mueller et al.¹⁰. In this experimental setup, membranes are
 51 prepared in the form of very thin lipid films. This method is suitable as a model of more complex natural
 52 membranes.^{11,12} Unlike CACO-2 or MDCK, which employ a monolayer of complex living cells, PAMPA
 53 and BLM methods both use simpler membranes that are unable to effect active transport (influx as well
 54 as efflux), paracellular transport, metabolism, or ion-trapping in lysosomes.^{13,14}

55 Experimental methods for the determination of membrane permeability have been supplemented by
 56 in-silico approaches, which can be divided into three main categories: molecular dynamics simulations,
 57 physics-based computational methods, and machine-learning statistical models.

58 Molecular dynamics (MD) simulations are *in silico* methods based on time-resolved simulations of
59 complex systems at the atomistic level¹⁵. We can derive many thermodynamic and kinetic properties of
60 the system from the MD simulations¹⁵. Thanks to the current level of computational power and
61 MD methods, we can now study the behavior of substances on membranes even at the atomic level¹⁶,
62 but they are so far limited by the quality of membrane force fields^{17,18}, long time scales necessary for
63 membrane permeation and hysteresis artefacts for advanced sampling methods¹⁹. Hence, the availability
64 of these data in large quantities is still quite limited, and MD is used more to model how molecules
65 permeate the membranes^{20,21}.

66 The PerMM²² and COSMOperm²³ are examples of physics-based calculated methods. PerMM is based
67 on the solubility diffusion model²⁴ and the positioning of proteins in membranes (PPM) method^{25,26}.
68 PerMM can also calculate the permeability coefficient across four types of membranes (DOPC, BLM,
69 CACO/MDCK, and BBB)²². COSMOperm is a mechanistic method for the prediction of membrane
70 permeability based on quantum chemical solubility calculations. Its basis is the calculation of the free
71 energy profile across the membrane. In general, this approach can calculate logPerm on any membrane.²³

72 Machine learning (ML) approaches are trained statistically over the existing experimental data, while
73 the data quality and size are extremely important. The QSAR (quantitative structure-activity
74 relationship) model is a mathematical model which identifies statistically significant correlations
75 between the structure of molecules and their properties, such as biological activity²⁷. The structure of
76 molecules is described by a variety of descriptors. Choosing the fitting descriptor is one of the key points
77 during the QSAR process. The history of QSAR is long, and countless various permeability QSAR
78 models have been developed, *e.g.* QSAR models for CACO-2 cell permeability²⁸, intestinal
79 permeability²⁹, blood-brain barrier (BBB)³⁰ and skin³¹, etc. QSAR models were recently generalized
80 with ML (machine-learning) models. These models are fitted to train data produced by experimental
81 methods. Experimental methods often used for the construction of these models are CACO-2 (*e.g.*, Wang
82 *et al.*³² or Frelund *et al.*³³) and PAMPA (*e.g.*, Sun *et al.*³⁴ or Gousiadou *et al.*³⁵). Sometimes these models
83 are created for a given type of molecule, *e.g.* cell-penetrating peptides³⁶ or macrocycles³⁷. As their
84 performance can be, in principle, only as good as the original data, we will not discuss them further here.

85 Because of the importance of permeability and the growing volume of published data obtained by
86 various methods, permeability data are available in well-established cheminformatics databases
87 (*e.g.*, PubChem³⁸ or ChEMBL³⁹). Nevertheless, these databases do not primarily focus on this type of
88 data, unlike the MolMeDB database.

89 MolMeDB⁴⁰ (<https://molmedb.upol.cz>) is a comprehensive, freely available database of membrane
90 interaction data, including permeation for small molecules. This database stores the manually obtained
91 data from scientific papers as well as the permeability data obtained from ChEMBL by data mining
92 workflow. Currently, there are more than 900,000 interactions for almost 500,000 molecules in
93 MolMeDB. Most of the data is permeability data from 56 theoretical or experimental methods on
94 48 various membranes.

95 This paper compares and interprets the results of four experimental methods – PAMPA, CACO-2,
96 MDCK, BLM/Liposomes, and two calculated – PerMM and COSMOperm – available in MolMeDB.
97 However, in order to understand this data properly, we must first understand the methods and their
98 constraints. Therefore, this paper has three main aims: (i) to compare methods with each other to put the
99 logPerm quantity in a real-world context, (ii) to identify and explain the limits of the mentioned methods,
100 and (iii) to put the logPerm quantity in a real-world context.

101

102 Methods

103 Data sources

104 Data was sourced from MolMeDB and ChEMBL. The data in ChEMBL was fetched by the ChEMBL
105 data web service. For this purpose, the KNIME⁴¹ semi-automatic workflow was created. This workflow
106 fetched information about molecules (SMILES, name, ChEMBL ID), publication (DOI), and
107 interactions. All interactions were converted to decimal logarithms, and all units of interactions were
108 converted to $\text{cm}\cdot\text{s}^{-1}$. Fetched data are available in MolMeDB. This data is labelled as ChEMBL in the
109 Secondary reference column in MolMeDB. The content of MolMeDB was exported as a .csv file. This
110 is possible on the website https://molmedb.upol.cz/stats/show_all.

111 Analysis of permeability data - MolMeDB data selection

112 Data was sourced from the MolMeDB database. The PAMPA method included methods that were
113 referred to as EPAM, EBAMP⁴²(for apparent PAMPA), and EPAMOL (for insintic PAMPA).The
114 BLM/liposomes included methods EBLM and ELIP in MolMeDB (for more details see:
115 <https://molmedb.upol.cz/browse/methods>).

116 In the cases of scatter plots (Fig.2and Fig. S1), a mean logPerm value for molecules that have more than
117 one logPerm value in MolMeDB was calculated. The mean values were calculated according to the rules
118 described in the Colab notebook. Cleveland dot plots (Fig. 4 A and B) is created from median values of
119 logPerm.

120 For greater inter-comparability of data, we excluded data other than that measured or calculated on the
121 cell membranes, generic membranes, and membranes of the intestine according to the MolMeDB
122 classification system (for more details, see: <https://molmedb.upol.cz/browse/membranes>). MolMeDB
123 stores permeability coefficients (logPerm) uniformly in the logarithmic form of $\text{cm}\cdot\text{s}^{-1}$.

124 Next, the dataset was narrowed down to data for small molecules ($MW \leq 800$ Da). For the computational
125 methods (PerMM and COSMOperm), interactions where the molecules were in a neutral state were
126 included, since only neutral form is usually eligible to penetrate the lipid membrane⁴³⁻⁴⁵. In the case of
127 experimental methods (CACO-2, MDCK, PAMPA, BLM/liposomes), only interactions for which the
128 pH was between 7.1 and 7.5 were included. Also, molecules with unknown pH were included. Only data
129 pertaining to a temperature of (20–25 °C) were included. 25 °C is the default temperature value in
130 MolMeDB. In the case of the data from ChEMBL, the value of temperature is unknown, and for this
131 reason, the approx. temperature of 25 °C is given in these cases. The resulting dataset contained data on
132 5483 interactions for 4218 unique molecules (by SMILES).

133 Analysis was done using KNIME workflow, and figures were created by R programming language
134 version 4.3.2⁴⁶ or by Python 3.10.12. The Colab notebook⁴⁷ for figures preparation is available on
135 MolMeDB GitHub (<https://github.com/MolMeDB/MolMeDB>), and the KNIMEworkflow is available
136 on WorkflowHub⁴⁸ (<https://workflowhub.eu/workflows/772>). The UpSet plot was created by UpSetR
137 Shiny App⁴⁹.

138 In the analyzed dataset, data originated from four different experimental methods – cell-based CACO-
139 2 (1415 molecules) and MDCK (402 molecules); membrane-based PAMPA (2592 molecules) and
140 BLM/liposomes (88 molecules); and two computational methods – PerMM (444 molecules) and
141 COSMOperm (504 molecules).

142

143 Apparent and intrinsic permeability

144 In order to compare and analyze values of permeability, we must be able to distinguish between two
145 concepts - apparent permeability and intrinsic (or molecular) permeability.

146 In a stirred container, the solute concentration is equalized in the bulk of the liquid. However, close to
147 the membrane surface, molecules only move by diffusion rather than by convection. As a solute flows
148 through the membrane, a concentration gradient builds up in close proximity to the membrane,
149 weakening the driving force.⁵⁰

150 According to equation 1, so-called measurable apparent permeability (p_{app}) is composed of
151 contributions:

152 p_{UWL} , $f_{neutral}$ and p_M .⁵¹

$$153 \quad \frac{1}{p_{app}} = \frac{1}{p_{UWL}} + \frac{1}{(f_{neutral} p_M)} \quad (1)$$

154 where p_{UWL} is the permeation through an unstirred water layer (UWL), $f_{neutral}$ is the fraction of molecule
155 that is in a non-ionized state in the donor compartment, and p_M is the molecule's intrinsic permeability.
156 This equation is plausible for the cases where the permeability of ionized species is negligible. That is
157 often valid, but there are specific examples when this assumption is not fulfilled^{52,53}. UWL is a static
158 layer of water directly adjacent to the surface of a membrane, acting as an additional resistance to
159 permeation. This value can vary with different stirring of donor and acceptor compartments, but for the
160 most common experimental setting of CACO-2/MDCK or PAMPA assay, this value is around -3.9 .¹³

161 Intrinsic permeability is often obtained from the calculation based on measuring the permeability scale
162 at different pH levels. This approach can be found in publications by Huque et al.⁵⁴, Avdeef et al.⁵⁵, or
163 Tsinman et al.⁵⁶. Furthermore, other implementations of this approach showed Velický et al.⁵⁷, where
164 the permeabilities are measured at different hydrodynamic regimes and from that, intrinsic permeability
165 can also be calculated.

166 Here, it can be noted that the apparent permeability is easily calculable from the intrinsic permeability
167 by taking into consideration the fraction of non-ionized molecules (from pK_a) and the permeation rate
168 through an unstirred water layer, which is specific to the experimental setup and can be determined from
169 data for fast-permeating molecules. Conversely, the determination of intrinsic permeability from the
170 apparent one is only feasible when the apparent permeability is not close to the diffusion limit. This
171 relation limits the usefulness of published apparent permeability data for intrinsic permeability models.

172

173 Results and discussion

174 Repeatability of the data

175 Firstly, we wanted to analyze the repeatability of the data to get the gist of the reported value variability
176 necessary to establish error estimation. For this purpose, permeability measurements for the same
177 molecules were considered using the same method at similar conditions (see Method section). The most
178 prevalent experimental method in the MolMeDB is PAMPA. We have taken seven most studied
179 molecules. They are listed in Table 1, along with the number of measured data points, average
180 permeability, and standard deviation.

181

182 **Table 1:** Molecules with the most data measured by the PAMPA method. Data taken from MolMeDB.
183 P_{intr} - number of intrinsic permeabilities, P_{app} - number of apparent permeabilities

	P_{intr}	P_{app}	Average LogPerm (cm/s)	Standard deviation (cm/s)	Minimum value (cm/s)	Maximum value (cm/s)
Antipyrine	1	6	-5.70	0.34	-6.09	-5.09
Carbamazepine	1	7	-4.83	0.65	-5.8	-3.89
Ketoprofen	1	12	-5.50	0.49	-6.39	-4.32
Naproxen	2	4	-4.38	1.62	-6.2	-1.69
Propranolol	3	14	-4.10	1.48	-6.68	-0.21
Theophylline	3	5	-5.94	0.78	-7.4	-5.07
Verapamil	3	6	-3.74	1.81	-5.19	-0.89

184

185 When visualizing the data from these seven molecules measured by PAMPA (Fig. 1), we see several
186 different behaviors of molecules, that can be discerned between intrinsic and apparent permeabilities.

187 Firstly, there are molecules with very low variance between measured values, such as antipyrine or
188 ketoprofen, within 0.5 log unit. Further molecules, such as carbamazepine or theophylline, have reasonable
189 variances within 1 log unit. The Table 1 shows several molecules with variance within 2 log units –
190 hence individual permeability measurements differ by more than 2 magnitudes. However, these large
191 errors can be explained by the mixing of apparent and intrinsic permeability, that Fig. 1 show to be
192 several log units different for those molecules.

193 Unfortunately, the information on whether intrinsic or apparent permeability is reported is not always
194 properly described in the literature or databases (e.g., we had to implement PAMPA P_{intr} into MolMeDB
195 upon preparation of this manuscript). The lack of distinction between apparent and intrinsic permeability
196 can lead to complications, especially when comparing data from multiple papers using the PAMPA
197 method.

198

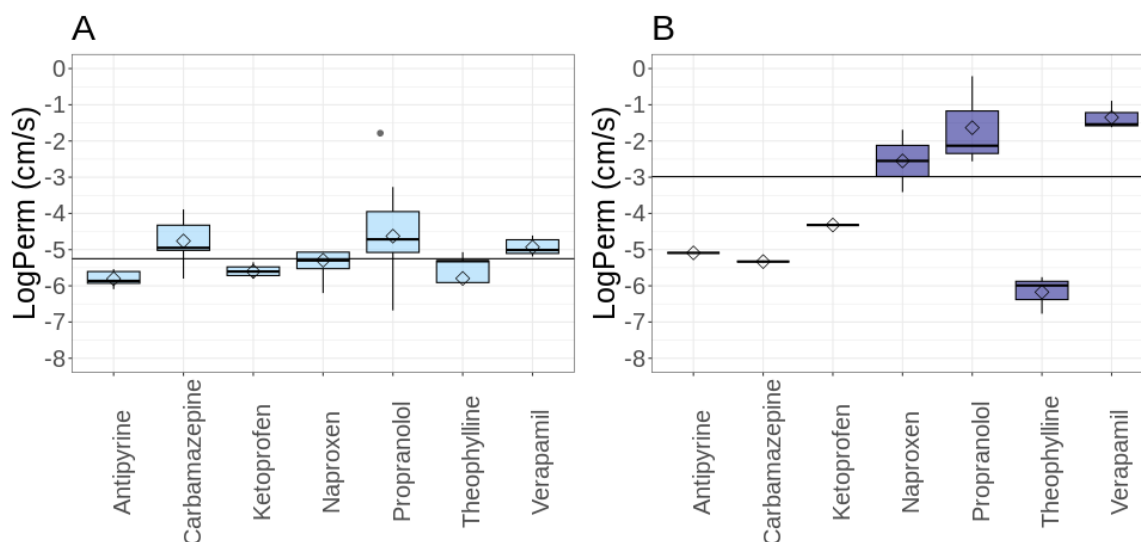


Fig. 1: Box plot of seven molecules with the most data measured by the PAMPA method (in MolMeDB). A – apparent permeability, B – intrinsic permeability. Rhombuses represent mean values of permeability, and the line corresponds to the median value of the dataset. Dots represent outliers.

199

200 A similar lack of information affects cell-based methods. There is crucial information about the direction
 201 of measurement or membrane transport proteins. There are two possible directions – either from apical
 202 to basolateral (from A to B) or from basolateral to apical (from B to A). The difference of permeabilities
 203 in direction can be large, e.g. in Colabufo et al.⁵⁸. The direction affects the value of measured
 204 permeability because these cells have an asymmetrical expression of pharmacologically relevant
 205 proteins that influence molecular transport.⁵⁹ These proteins are (i) efflux transporters,
 206 e.g., P-glycoprotein (MDR1, ABCB1), MRP2 (ABCC2) or BCRP (ABCG2), and (ii) uptake proteins,
 207 e.g., OCT2 (SLC22A2), OATP2B1 (SLCO2B1), or PEPT1 (SLC15A1)^{59,60}. In the case of these
 208 measurements, not only the direction in which the permeability is measured but also the presence of
 209 transporter inhibitors plays a role^{33,59}. The inhibitors increase the permeability of substrates of efflux
 210 transporters³³. Gene knockout techniques can also alter the expression of these transporters in the cells⁶⁰.
 211 Unfortunately, this information is often not sufficiently reported together with permeability data in the
 212 public available databases.

213 Comparison of methods

214 In this analysis, we have studied the correlation between each pair of permeability methods to see how
 215 they can be supplemented with each other if needed. A mean logPerm value for each molecule and
 216 method was calculated, and for molecules that were measured/calculated by at least two methods, these
 217 data were compared. The comparison of all possible pairs of methods is available in Supporting
 218 Information (Fig. S1). Here, we discuss the most prominent and illustrious examples.

219 The first finding is the strong correlation ($R^2 = 0.82$) between CACO-2 and MDCK (Fig. 2A). This
 220 correlation is expected because both methods are cell-based methods, and their strong correlation was
 221 described by Irvine et al.³

222 From the previous section, we know the PAMPA dataset contains a mixture of apparent and intrinsic
 223 permeabilities that need to be differentiated if the data are to be compared. Fig. 2B is the correlation

224 among CACO-2 & MDCK vs intrinsic PAMPA. This correlation is very weak ($R^2 = 0.03$) because, in
225 contrast to PAMPA, the CACO-2 and MDCK methods can provide only apparent permeability. On the
226 other hand, Fig. 2C shows the correlation ($R^2 = 0.44$) between CACO-2 & MDCK vs apparent PAMPA.
227 This correlation is unsurprisingly stronger because the PAMPA apparent permeabilities correlate well
228 with CACO-2 and MDCK data. This observation is consistent with the literature because the correlation
229 among these methods was already described in the literature (PAMPA and CACO-2 were described by
230 Zhu et al.⁶¹, MDCK and PAMPA were published by von Richter et al.⁶²). However, in addition to the
231 membranes, the cell-based methods CACO-2 and MDCK also have membrane transport proteins, which
232 can influence the transport of molecules through the membrane, and thus lower the correlation.
233 However, the correlation between CACO-2 and PAMPA and MDCK and PAMPA indicates passive
234 diffusion as a dominant transport mechanism in the case of both cell monolayers^{11,63}. A good correlation
235 between CACO-2 & MDCK vs apparent PAMPA can indicate a smaller role of membrane transporters
236 in this dataset.

237 Fig. 2D shows a strong correlation ($R^2 = 0.73$) between the calculated methods (PerMM and
238 COSMOperm) and BLM / liposomes (abbreviated “BLM”). The BLM method is a very important
239 experimental method because, in contrast to other experimental methods, the BLM is the diffusion-
240 unlimited method. Thus, molecular permeability is easily determined using BLM. The BLM is not
241 widespread, and therefore, we do not have as much data available as the PAMPA method.

242 The authors of both calculated methods validated these methods against BLM experimental data^{22,23}.
243 Bittermann et al.⁶⁴ report that COSMOperm has RMSE = 0.62 log units for neutral molecules and RMSE
244 = 0.7 log units for ions. The PerMM method has RMSE = 1.15 log unit by Lomize et al.²². Therefore, it
245 is no surprise that these methods correlate strongly. In addition, highly similar BLM datasets were used
246 for validation, and this validation data comprises the majority of the BLM data in the MolMeDB
247 database. We also see that the values are wide ranged because BLM, COSMOperm, and PerMM are
248 methods that are not constrained by diffusion limits and provide intrinsic permeabilities.

249 Fig. 2E is a correlation between calculated (PerMM and COSMOperm) ($R^2 = 0.58$). This correlation is
250 not surprising, given what has been said about these methods above. Both methods are unlimited by
251 diffusion limit and can predict intrinsic permeabilities.

252 Fig. 2F is an example of the weak correlation between diffusion-limited method (PAMPA) and -
253 unlimited method (PerMM). More examples can be found in Supporting information (Fig. 1S H and O).
254 As we can clearly see, PAMPA data are located in the range of values (approx. from -8 to 4 log units),
255 but the PerMM method is in the wider range of values (approx. from -16 to 4). Differences between the
256 logPerm values from PerMM and PAMPA can be huge (several log units), although the PerMM method
257 was successfully evaluated by PAMPA-DS (PAMPA-DS: $R^2 = 0.75$, RMSE = 1.59 log unit) by Lomize
258 et al.²². Our correlation is weaker ($R^2 = 0.27$) than Lomize’s because our dataset contains apparent
259 permeabilities and intrinsic permeabilities, whereas Lomize used only intrinsic permeabilities from one
260 source.

261 Apart from the correlation, it is often more useful to calculate mean absolute error (MAE) for each
262 comparison (Table 2). It shows that the closest pair of methods are both cell-based methods (CACO-2
263 and MDCK) followed by their pairs with their membrane-based counterpart sharing similar range –
264 apparent PAMPA. The error between BLM and both computational methods is comparable to the MAE
265 in between them, but their similarity to cell-based methods is weak with the largest error. As a negative
266 control, we have tried mean predictor, i.e. we calculated MAE of each method towards the mean average
267 value calculated on its dataset. This value serves as a negative control for the fit to that dataset. If the
268 MAE value for pair is lower or at least similar than MAE to mean predictor, then it can be combined.
269 This comparison has shown that we can combine both cell-based methods (CACO-2 and MDCK)
270 together with apparent PAMPA. Similarly, both computed physics-based methods (COSMOperm and

271 PerMM) can be used to predict membrane-based BLM method and to some extent also to intrinsic
272 PAMPA.

273

274 **Table 2.** Mean absolute errors (MAE) for each pair of methods. Colors define indicate the ranges – green
275 has MAE range < 1 log units, yellow has MAE range between 1 and 3 log units, and red has MAE range
276 > 3 log units. Diagonal shows MAE of mean predictor, i.e. towards mean average value of each dataset.
277 This value serves as a negative control for the fit to that dataset. If the MAE value for pair is lower or at
278 least similar than MAE to mean predictor, then the datasets can be combined.

MAE	CACO	MDCK	PAMPA app.	PAMPA intr.	BLM	COSMO perm	PerMM
CACO	0.72	0.34	0.73	2.81	2.39	2.79	4.02
MDCK	0.34	0.65	0.74	2.00	3.49	2.76	3.34
PAMPA app.	0.73	0.74	0.85	2.53	3.30	3.56	3.95
PAMPA intr.	2.81	2.00	2.53	1.59	3.26	1.78	2.44
BLM	2.39	3.49	3.30	3.26	1.90	0.97	1.42
COSMO perm	2.79	2.76	3.56	1.78	0.97	1.71	1.98
PerMM	4.02	3.34	3.95	2.44	1.42	1.98	3.11

279

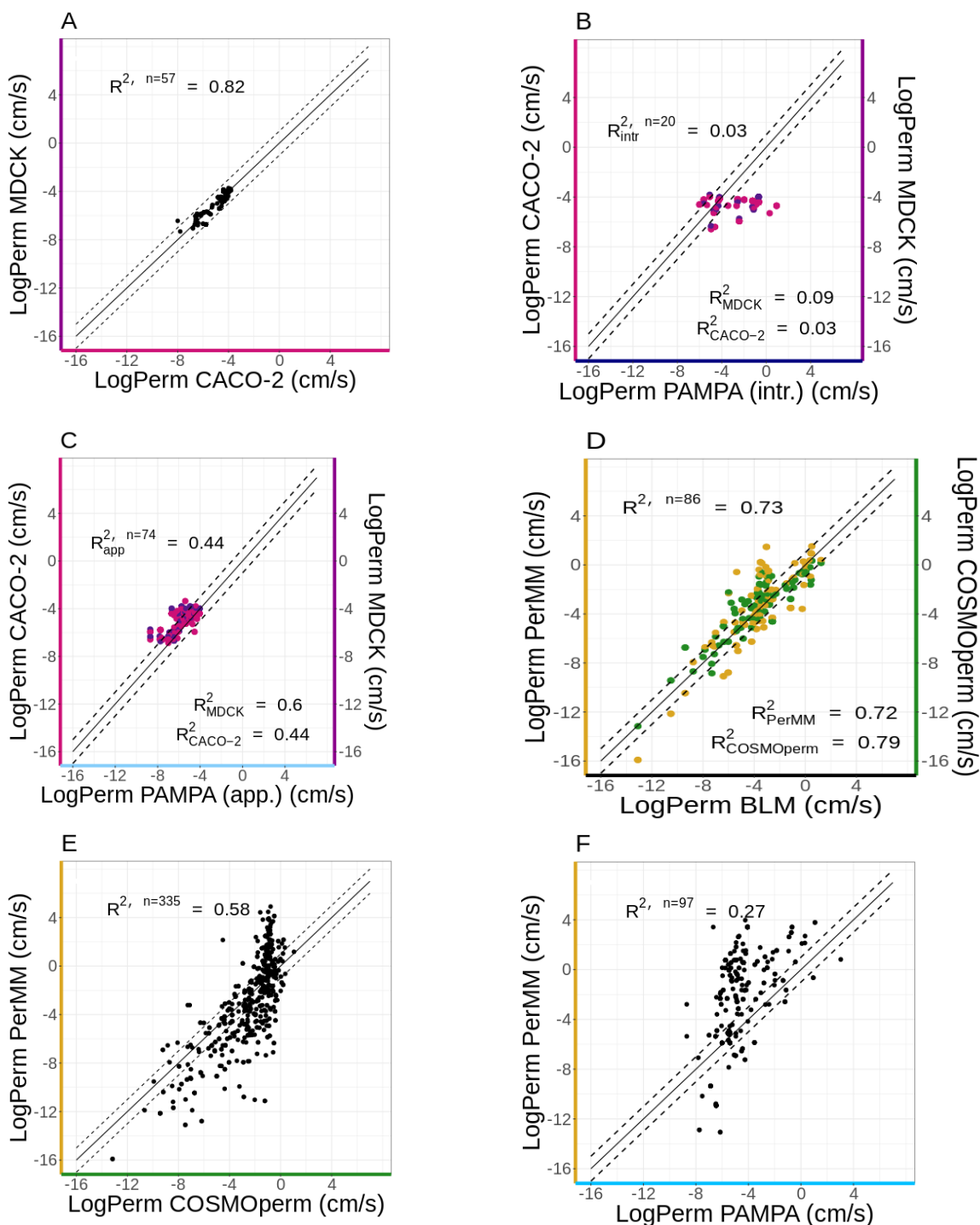
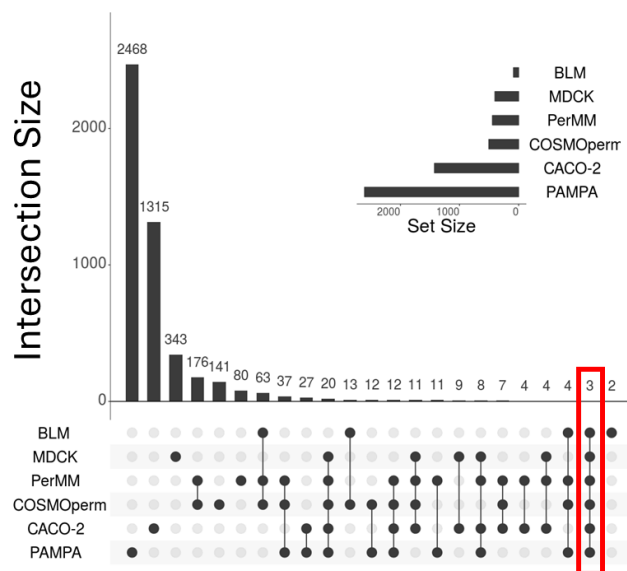


Fig. 2: Mean logPerM values of molecules that are present in overlaps between A: CACO-2 and MDCK datasets; B: CACO-2 & MDCK and intrinsic PAMPA datasets, C: CACO-2 & MDCK and apparent PAMPA datasets D: COSMOperm & PerMM and BLM/Liposomes datasets, E: PerMM and COSMOperm datasets, F: PerMM and PAMPA datasets (apparent and intrinsic permeabilities). The solid line represents the parity of permeation values, and the dashed lines represent a logPerM difference of ± 1 between methods. All data is displayed in a log of $\text{cm}\cdot\text{s}^{-1}$. N is the number of unique molecules in overlap, and R^2 is the coefficient of determination.

280 Overlaps of the methods

281 All the above-mentioned methods are well-known, and the permeabilities of small molecules determined
282 by these methods have been published in many publications.

283 The UpSet plot (Fig. 3) shows overlap between all six methods by molecules (MolMeDB IDs). The
284 biggest overlap is between both calculated methods (176 molecules); the second biggest one is the
285 overlap among PerMM, COSMOperm, and BLM (63 molecules), and all other overlaps are much
286 smaller.



287

Fig. 3: Upset plot of six methods (created with UpSetR Shiny App). Columns in the graph represent a number of molecules that were measured by the combination of methods shown by black circles only. The first column shows molecules that were measured by PAMPA only, and the last column shows molecules that were measured by PAMPA, calculated by PerMM but which are not present in any other dataset. This figure includes only intersections with more than one molecule. The overlap among all six methods is highlighted by red rectangle.

288

289 Overlap among all six methods contains three well-known drugs (hydrocortisone, salicylic acid, and
290 acetylsalicylic acid). Fig. 4A is the Cleveland dot plot of logPerm median values from individual
291 methods for each of these molecules. Fig. 4B shows median permeability values for molecules that are
292 present in all datasets except BLM due to the low number of molecules in the BLM/liposome dataset.
293 The data shown in Fig. 4 underline the phenomena from the previous chapter. MDCK, CACO-2, and
294 apparent PAMPA (purple, pink, and light blue points) often give very similar results. In the case of
295 atenolol, verapamil, or warfarin, the difference between apparent PAMPA (light blue points) and
296 intrinsic PAMPA (navy blue points) can be huge. Also, the figure demonstrates the variability of logPerm
297 values from all calculated methods (green and yellow points).

298

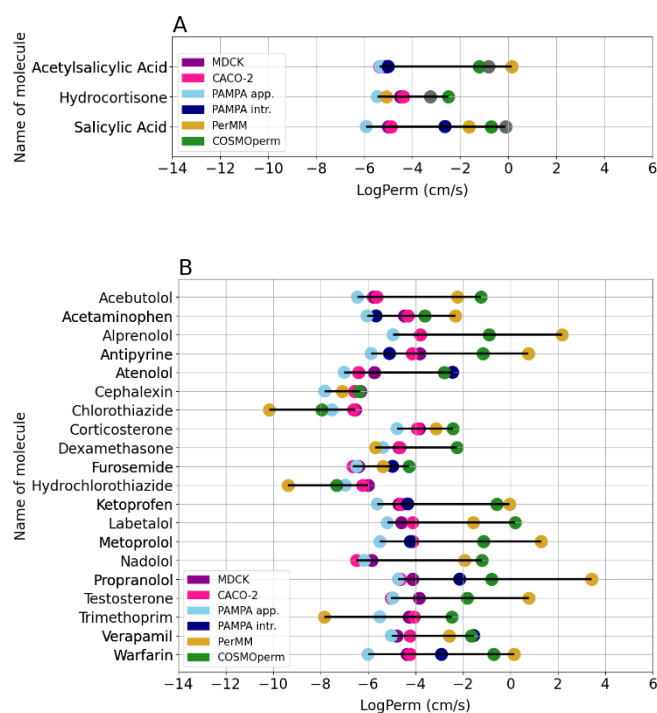


Fig. 4: Cleveland dot plot of median permeability coefficients for molecules in the overlap of MDCK, CACO-2, PAMPA, BLM / Liposomes, COSMOperm, and PerMM datasets.

299

300 The limits of permeability of the compared methods

301 Distributions of values for individual methods have shown that each method has some limits of reported
 302 permeability that differ. Fig. 5 shows that almost all CACO-2 and MDCK experimental values fall in a
 303 fairly narrow range from -8 to -4 log units. The lower limit is probably due to the duration of the
 304 experiments. It is hard to measure slower permeation in experimental conditions within ambient times.
 305 The upper limit (around -3.9) corresponds to the diffusion limit through an unstirred water layer
 306 (UWL),¹³ as explained above. Here, it can be noted that at least 40% of molecules studied using CACO-
 307 2 or MDCK assays were close to this diffusion limit. Therefore, a significant amount of measured
 308 permeability is, in fact, diffusion of the unstirred water layer, and their intrinsic permeability is thus
 309 anywhere between -4 and 4 . However, for example Stenberg et al, published CACO-2 data where they
 310 tried to reduce the effect of UWL on permeability by stirring⁶⁵.

311 Data from the PAMPA experimental assay (Fig. 5 PAMPA) has a visible peak around $\log\text{Perm} = -4$,
 312 though higher permeation rates were also measured. This phenomenon is again caused by the above-
 313 mentioned mixture of apparent and intrinsic PAMPA permeabilities in the literature. Some publications
 314 (e.g. refs. ^{63,66,67}) report the apparent permeability as a direct experimental value of permeation, which
 315 is related to CACO-2 permeability. On the other hand, other publications of PAMPA permeation data
 316 (e.g. refs. ^{54,55}) report the intrinsic permeability, thus mixing permeability values. As can be seen from
 317 the figure, the apparent permeability (light blue) peaks between the values -8 and -4 , while the intrinsic
 318 permeability (navy blue) is shifted to higher values. However, some values of apparent permeability are
 319 over -4 threshold. This phenomenon can be explained by e.g. effort to reduce the UWL layer in
 320 permeability assay by increasing of stirring speed⁶⁸. Fujikawa et al present e.g. for Desipramine $\log\text{Perm}$
 321 $= -4.77$ (0 rpm), $\log\text{Perm} = -4.00$ (200 rpm), and $\log\text{Perm} = -3.81$ (250 rpm)⁶⁷.

322 Permeabilities measured by the BLM/liposome method are typically higher than -4 , likely due to the
323 relatively large membrane area in liposomal systems. Although the BLM/liposome method also provides
324 apparent permeabilities, the UWL, in this case, is significantly smaller than that of CACO-2, MDCK or
325 PAMPA, and its contribution is practically negligible. The lowest experimentally measured permeability
326 value is -13.1 log units for saccharose from Brunner et al.⁶⁹. Its authors say that any value lower than
327 -10 log unit is hardly measurable.

328 With the computational approaches – PerMM and COSMOPerm (Fig. 5 PerMM and COSMOPerm), we
329 observe a broad distribution of permeation rates from very slow permeation ($\log\text{Perm} \leq -8 \text{ cm}\cdot\text{s}^{-1}$) to
330 very fast permeation ($\log\text{Perm} \geq -4 \text{ cm}\cdot\text{s}^{-1}$). This is typical for calculated methods because they have
331 no experimental limits. We can compare the result from the experimental method with the result from
332 the calculation, but only up to the limits of the experimental methods. Beyond these limits, there is no
333 possibility of comparison. The permeabilities obtained by these calculated methods can be categorized
334 as intrinsic permeabilities.

335 In addition, it is interesting to mention differences in averages of octanol/water partition coefficient
336 (LogP) and molecular weight (MW) for different methods.

337 CACO-2, MDCK, and PAMPA have considerably higher averages of both values than the other three
338 methods. This is probably caused by the fact that most of the permeating molecules measured in these
339 assays in scientific publications are drug-like molecules, and the molecular weight of around 400 Da
340 and logP around 3 corresponds to a typical drug candidate.

341 BLM/liposome methods have much lower MW and logP (MW = 159.4 Da, logP = 0.3). This is probably
342 because these methods are not commonly used for extensive drug candidate molecule assays; rather,
343 there are only a few measurements of typical small molecules (e.g., benzoic acid). These data are then
344 often used as training/validation of different computational methods since they are not influenced by the
345 -8 and -4 thresholds that are hard (or even impossible) to overcome for other experimental methods.

346 Computational methods (COSMOPerm, PerMM) can predict the permeabilities of a wide range of
347 molecules. Their average LogP of around 1.8 and MW of around 260 Da is lower than for experimental
348 methods. This has at least two co-occurring reasons. Firstly, using computational methods, it is possible
349 to calculate small molecules (oxygen, water, carbon dioxide) that are commonly not measured in
350 permeation assays. Secondly, the calculation difficulty scales with molecular weight, and therefore, it is
351 more expensive to calculate molecules with larger MW.

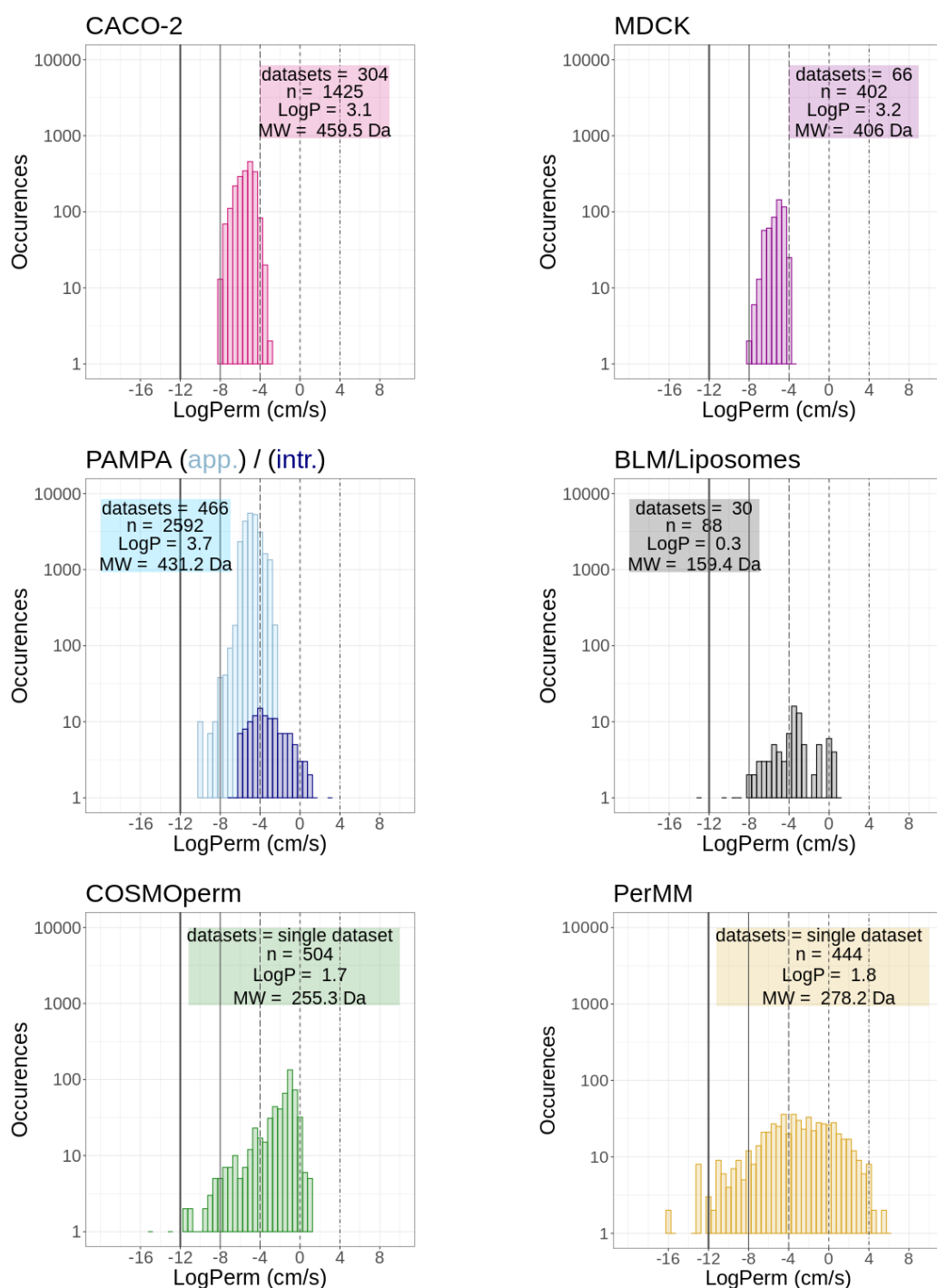


Fig. 5: Distribution of selected LogPerm values (uncharged molecules, 25 °C, smaller than 800 Da) from MolMeDB database according to selected methods. Datasets – number of unique datasets (by primary reference), LogP – mean logP of unique molecules, MW – mean molecular weight of unique molecules, n - number of unique molecules (by SMILES) in combined datasets. All data is displayed in a log of cm/s, bin size = 0.5. The vertical lines emphasize values -12, -8, -4, 0, +4, as discussed above. Occurrences are in log scale.

354 Interpreting permeability coefficients real-world time scales

355 For the interpretation of the limits we observed within the previous sections, we have designed several
356 simplified boundaries as a multiplication of 4 log units, that can help to explain the limitations of
357 permeability coefficients in real world examples of the time scale for permeation events (Fig. 6).

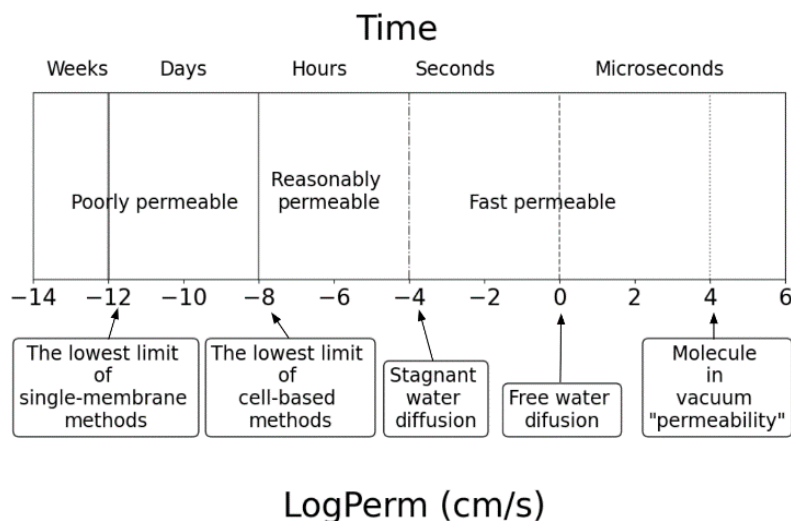


Fig. 6: Illustration of permeability coefficients in the context of timescale

358 The lowest experimental value of logPerm is -13.1 log units in our dataset (Fig 3 BLM/liposomes)⁶⁹.
359 Hence, the first line of logPerm around -12 log units corresponds to the lowest permeation rates still
360 measurable by single-membrane experimental methods. It is close to the practical limit of the slowest
361 passive permeation that still results in a biologically feasible amount of e.g. highly toxic compounds
362 permeating over a physiologically relevant amount of time. For a permeation area equal to that of an
363 entire human intestine (30 m^2)⁷⁰ and 0.1 L as a volume of the intestinal fluid,⁷¹ only 0.25% of a permeant
364 will have permeated in ten days at such rate with logPerm = -12 log units.

365 The second line is logPerm around -8 log units. This area corresponds to the lowest limit of cell-based
366 methods (e.g., CACO-2 or MDCK) as well as PAMPA. With the typical measurement setup for these
367 measurements (donor volume 0.5 mL , permeation area 1.4 cm^2),⁷² the compound with logPerm = -8 log
368 units will permeate approx. 2% of the permeant in 10 days. The same limit is observable in, e.g. Deur
369 et al.⁷³ for CACO-2, Chiba et al.⁷⁴ for MDCK, or Flaten et al.⁷⁵ for PAMPA.

370 The third important value of logPerm is -4 log units. This represents the value of -3.9 log unit that
371 corresponds to the effect of an unstirred water layer (UWL) as we already discussed earlier in previous
372 section. Hence the typical permeability coefficient values will fall in between logPerm -8 to -4 log
373 units.

374 Fourth line of logPerm around 0 log units relates to an unrestrained diffusion in water and represents the
375 maximum permeability measurable by experimental methods in water medium. Such logPerm values
376 correspond to the permeation of molecules through water slice of similar thickness to membrane, where
377 there is no energy barrier for permeation and diffusion coefficient is equal to the water self-diffusion
378 coefficient. Then, the homogeneous solubility model for the permeation coefficient is valid:

$$379 \quad P = \frac{K \cdot D}{L} \quad (2)$$

380 where K is the partition coefficient between the membrane and water phase (considered equal to 1, if
381 there is no extra partitioning into the slice due to no energy barrie), D is the diffusion coefficient

382 ($3 \times 10^{-9} \text{ m}^2/\text{s}$ for water self-diffusion, taken from ref. ⁷⁶), and L is the thickness of the membrane (the
383 thinnest experimentally possible membrane with a thickness around 4 nm). Then, P is 75 cm/s, and
384 $\log \text{Perm}$ is +1.9 log units. Since drugs are bigger molecules than water, they usually have diffusion
385 constant lower by order of magnitude or more (e.g., ibuprofen has $D = 5.5 \times 10^{-10} \text{ m}^2/\text{s}$)⁷⁷, we have set
386 this simplified limit to 0 log unit.

387 The rightmost highlighted value of $\log \text{Perm}$ is around +4 log units. This value of $\log \text{Perm}$ presents the
388 theoretical upper limit of permeability, describing an unrestrained molecule travelling through a vacuum
389 (together with a spherical chicken from classical physics joke). This was calculated using the formula
390 for the root mean square velocity of a gas molecule (equation 3):

$$391 \quad v = \text{sqrt}(3kT/m) \quad (3)$$

392 Where k is the Boltzmann constant, T is the temperature (K), and m is the mass of the molecule. If we
393 assume the mass of the molecule as $200 \text{ g} \cdot \text{mol}^{-1}$ and a temperature of $37 \text{ }^\circ\text{C}$, we get a velocity of
394 $6000 \text{ m} \cdot \text{s}^{-1}$, which can be considered as a gas permeability limit ($\log \text{Perm} = +5.8 \text{ log units of } \text{cm} \cdot \text{s}^{-1}$)
395 but only in the case of a negligible thickness of the membrane, area of permeation equal to the projection
396 is of the molecule itself and maximum possible concentration difference. This value is purely
397 hypothetical and does not correspond to the biomembrane permeability in real liquid conditions. It is
398 only stated here as the absolute upper limit of the permeability. Even the 60 times smaller value of
399 permeability ($\log \text{Perm} = +4 \text{ log units of } \text{cm} \cdot \text{s}^{-1}$) is still purely hypothetical and impossible to get in
400 biomembrane permeation; thus, this limit is used in graphs and discussion below due to the 4 orders of
401 magnitude difference between all other limits.

402 Conclusions

403 In summary, we have meta-analyzed a large amount of permeability data from freely available databases
404 MolMeDB and ChEMBL. Permeability is, among other things, the basis of classifying drug substances
405 into the Biopharmaceutics Classification System (BCS)⁷⁸ and this classification forms the basis of
406 product formulation and regulatory approval strategy decisions, hence it is important to have reliable
407 data for permeability. Moreover, permeability as an important pharmacological property is of interest to
408 many researchers who try to create machine learning algorithms for its prediction. The variability
409 between individual measurements, even for the same methods, has shown that efforts should be made
410 to develop robust methods that would enable consistent inter-laboratory values to be measured and
411 stored in FAIR manner, e.g. in MolMeDB database. Next the analysis of individual methods observed
412 their data limits. Meta-analysis in-between the datasets has shown that cell-based methods such as
413 CACO-2, MDCK are comparable with apparent PAMPA, but all of these methods correlate less with
414 calculated physics-based methods (COSMOperm and PerMM) and with single membrane-based
415 BLM/liposomes or intrinsic PAMPA, which are based on molecular permeabilities. This needs to be
416 considered when permeability data are from different methods compared or used in machine-learning
417 approaches. Finally, we have devised a scale with five significant permeability values as a multiplier of
418 4 log units of $\text{cm} \cdot \text{s}^{-1}$ to help a comprehensive understanding of the permeability data within their
419 physical context.

420

421 Author Contributions

422 K.S. – data analysis, data curation, visualization, manuscript writing M.B. – data analysis, data
423 interpretation, manuscript writing, J.J. – MolMeDB development, data curation, F.Š. - conceptualization,
424 funding acquisition, manuscript writing, K.B. – conceptualization, funding acquisition, manuscript
425 writing.

426

427 Conflicts of interest

428 There are no conflicts to declare.

429

430 Acknowledgements

431 We acknowledge the help of Adam Tywoniak in carefully reading the manuscript. The project was
432 supported by the Czech Grant Agency project GAČR 24-11986S. K.S. and K.B. acknowledge support
433 from Palacky University Olomouc Project IGA_PrF_2024_017. K.B. and J.J. acknowledge support
434 from the ELIXIR-CZ infrastructure (Project LM2023055). The graphical abstract also includes icons
435 adapted from Bioicons.com (<https://bioicons.com/>).

436 References

- 437 (1) Di, L.; Artursson, P.; Avdeef, A.; Benet, L. Z.; Houston, J. B.; Kansy, M.; Kerns, E. H.; Lennernäs, H.; Smith, D. A.; Sugano,
438 K. The Critical Role of Passive Permeability in Designing Successful Drugs. *ChemMedChem* **2020**, *15* (20), 1862–1874.
439 <https://doi.org/10.1002/cmdc.202000419>.
- 440 (2) Hidalgo, I. J.; Raub, T. J.; Borchardt, R. T. Characterization of the Human Colon Carcinoma Cell Line (Caco-2) as a Model
441 System for Intestinal Epithelial Permeability. *Gastroenterology* **1989**, *96* (3), 736–749.
- 442 (3) Irvine, J. D.; Takahashi, L.; Lockhart, K.; Cheong, J.; Tolan, J. W.; Selick, H. E.; Grove, J. R. MDCK (Madin-Darby Canine
443 Kidney) Cells: A Tool for Membrane Permeability Screening. *Journal of Pharmaceutical Sciences* **1999**, *88* (1), 28–33.
444 <https://doi.org/10.1021/js9803205>.
- 445 (4) Fedi, A.; Vitale, C.; Ponschin, G.; Ayehunie, S.; Fato, M.; Scaglione, S. In Vitro Models Replicating the Human Intestinal
446 Epithelium for Absorption and Metabolism Studies: A Systematic Review. *Journal of Controlled Release* **2021**, *335*,
447 247–268. <https://doi.org/10.1016/j.jconrel.2021.05.028>.
- 448 (5) Kansy, M.; Senner, F.; Gubernator, K. Physicochemical High Throughput Screening: Parallel Artificial Membrane
449 Permeation Assay in the Description of Passive Absorption Processes. *J. Med. Chem.* **1998**, *41* (7), 1007–1010.
450 <https://doi.org/10.1021/jm970530e>.
- 451 (6) Bermejo, M.; Avdeef, A.; Ruiz, A.; Nalda, R.; Ruell, J. A.; Tsinman, O.; González, I.; Fernández, C.; Sánchez, G.; Garrigues,
452 T. M.; Merino, V. PAMPA—a Drug Absorption in Vitro Model. *European Journal of Pharmaceutical Sciences* **2004**, *21*
453 (4), 429–441. <https://doi.org/10.1016/j.ejps.2003.10.009>.
- 454 (7) Di, L.; Kerns, E. H.; Fan, K.; McConnell, O. J.; Carter, G. T. High Throughput Artificial Membrane Permeability Assay for
455 Blood–Brain Barrier. *European Journal of Medicinal Chemistry* **2003**, *38* (3), 223–232. [https://doi.org/10.1016/S0223-5234\(03\)00012-6](https://doi.org/10.1016/S0223-5234(03)00012-6).
- 456 (8) Ottaviani, G.; Martel, S.; Carrupt, P.-A. Parallel Artificial Membrane Permeability Assay: A New Membrane for the Fast
457 Prediction of Passive Human Skin Permeability. *J. Med. Chem.* **2006**, *49* (13), 3948–3954.
458 <https://doi.org/10.1021/jm060230t>.
- 459 (9) Henriques, P.; Bicker, J.; Silva, S.; Doktorovová, S.; Fortuna, A. Nasal-PAMPA: A Novel Non-Cell-Based High Throughput
460 Screening Assay for Prediction of Nasal Drug Permeability. *International Journal of Pharmaceutics* **2023**, *643*, 123252.
461 <https://doi.org/10.1016/j.ijpharm.2023.123252>.
- 462 (10) Mueller, P.; Rudin, D. O.; Ti Tien, H.; Wescott, W. C. Reconstitution of Cell Membrane Structure in Vitro and Its
463 Transformation into an Excitable System. *Nature* **1962**, *194* (4832), 979–980. <https://doi.org/10.1038/194979a0>.
- 464 (11) Sugano, K.; Kansy, M.; Artursson, P.; Avdeef, A.; Bendels, S.; Di, L.; Ecker, G. F.; Faller, B.; Fischer, H.; Gerebtzoff, G.;
465 Lennernaes, H.; Senner, F. Coexistence of Passive and Carrier-Mediated Processes in Drug Transport. *Nat Rev Drug*
466 *Discov* **2010**, *9* (8), 597–614. <https://doi.org/10.1038/nrd3187>.
- 467 (12) Winterhalter, M. Black Lipid Membranes. *Current Opinion in Colloid & Interface Science* **2000**, *5* (3–4), 250–255.
468 [https://doi.org/10.1016/S1359-0294\(00\)00063-7](https://doi.org/10.1016/S1359-0294(00)00063-7).
- 469 (13) Bittermann, K.; Goss, K.-U. Predicting Apparent Passive Permeability of Caco-2 and MDCK Cell-Monolayers: A
470 Mechanistic Model. *PLoS ONE* **2017**, *12* (12), e0190319. <https://doi.org/10.1371/journal.pone.0190319>.
- 471 (14) Berben, P.; Bauer-Brandl, A.; Brandl, M.; Faller, B.; Flaten, G. E.; Jacobsen, A.-C.; Brouwers, J.; Augustijns, P. Drug
472 Permeability Profiling Using Cell-Free Permeation Tools: Overview and Applications. *European Journal of*
473 *Pharmaceutical Sciences* **2018**, *119*, 219–233. <https://doi.org/10.1016/j.ejps.2018.04.016>.
- 474 (15) Padhi, A. K.; Janežič, M.; Zhang, K. Y. J. Molecular Dynamics Simulations: Principles, Methods, and Applications in
475 Protein Conformational Dynamics. In *Advances in Protein Molecular and Structural Biology Methods*; Elsevier, 2022;
476 pp 439–454. <https://doi.org/10.1016/B978-0-323-90264-9.00026-X>.
- 477 (16) Guo, J.; Bao, Y.; Li, M.; Li, S.; Xi, L.; Xin, P.; Wu, L.; Liu, H.; Mu, Y. Application of Computational Approaches in
478 Biomembranes: From Structure to Function. *WIREs Comput Mol Sci* **2023**, e1679. <https://doi.org/10.1002/wcms.1679>.
- 479 (17) Paloncýová, M.; Fabre, G.; DeVane, R. H.; Trouillas, P.; Berka, K.; Otyepka, M. Benchmarking of Force Fields for
480 Molecule–Membrane Interactions. *J. Chem. Theory Comput.* **2014**, *10* (9), 4143–4151.
481 <https://doi.org/10.1021/ct500419b>.
- 482

- 483 (18) Kiirikki, A. M.; Antila, H. S.; Bort, L. S.; Buslaev, P.; Favela-Rosales, F.; Ferreira, T. M.; Fuchs, P. F. J.; Garcia-Fandino, R.;
484 Gushchin, I.; Kav, B.; Kučerka, N.; Kula, P.; Kurki, M.; Kuzmin, A.; Lalitha, A.; Lolicato, F.; Madsen, J. J.; Miettinen, M. S.;
485 Mingham, C.; Monticelli, L.; Nencini, R.; Nesterenko, A. M.; Piggot, T. J.; Piñeiro, Á.; Reuter, N.; Samantray, S.; Suárez-
486 Lestón, F.; Talandashti, R.; Ollila, O. H. S. Overlay Databank Unlocks Data-Driven Analyses of Biomolecules for All. *Nat*
487 *Commun* **2024**, *15* (1), 1136. <https://doi.org/10.1038/s41467-024-45189-z>.
- 488 (19) Lichtinger, S. M.; Biggin, P. C. Tackling Hysteresis in Conformational Sampling: How to Be Forgetful with MEMENTO. *J.*
489 *Chem. Theory Comput.* **2023**, *19* (12), 3705–3720. <https://doi.org/10.1021/acs.jctc.3c00140>.
- 490 (20) Palonciová, M.; DeVane, R. H.; Murch, B. P.; Berka, K.; Otyepka, M. Rationalization of Reduced Penetration of Drugs
491 through Ceramide Gel Phase Membrane. *Langmuir* **2014**, *30* (46), 13942–13948. <https://doi.org/10.1021/la503289v>.
- 492 (21) Palonciová, M.; Vávrová, K.; Sovová, Ž.; DeVane, R.; Otyepka, M.; Berka, K. Structural Changes in Ceramide Bilayers
493 Rationalize Increased Permeation through Stratum Corneum Models with Shorter Acyl Tails. *J. Phys. Chem. B* **2015**,
494 *119* (30), 9811–9819. <https://doi.org/10.1021/acs.jpcc.5b05522>.
- 495 (22) Lomize, A. L.; Pogozheva, I. D. Physics-Based Method for Modeling Passive Membrane Permeability and Translocation
496 Pathways of Bioactive Molecules. *J. Chem. Inf. Model.* **2019**, *59* (7), 3198–3213.
497 <https://doi.org/10.1021/acs.jcim.9b00224>.
- 498 (23) Schwöbel, J. A. H.; Ebert, A.; Bittermann, K.; Huniar, U.; Goss, K.-U.; Klamt, A. COSMO *Perm*: Mechanistic Prediction of
499 Passive Membrane Permeability for Neutral Compounds and Ions and Its pH Dependence. *J. Phys. Chem. B* **2020**, *124*
500 (16), 3343–3354. <https://doi.org/10.1021/acs.jpcc.9b11728>.
- 501 (24) Diamond, J. M.; Katz, Y. Interpretation of Nonelectrolyte Partition Coefficients between Dimyristoyl Lecithin and
502 Water. *J. Membr. Biol.* **1974**, *17* (1), 121–154. <https://doi.org/10.1007/BF01870176>.
- 503 (25) Lomize, A. L.; Pogozheva, I. D.; Mosberg, H. I. Anisotropic Solvent Model of the Lipid Bilayer. 2. Energetics of Insertion
504 of Small Molecules, Peptides, and Proteins in Membranes. *J. Chem. Inf. Model.* **2011**, *51* (4), 930–946.
505 <https://doi.org/10.1021/ci200020k>.
- 506 (26) Lomize, A. L.; Pogozheva, I. D.; Lomize, M. A.; Mosberg, H. I. Positioning of Proteins in Membranes: A Computational
507 Approach. *Protein Science* **2006**, *15* (6), 1318–1333. <https://doi.org/10.1110/ps.062126106>.
- 508 (27) Sprous, D. G.; Palmer, R. K.; Swanson, J. T.; Lawless, M. QSAR in the Pharmaceutical Research Setting: QSAR Models
509 for Broad, Large Problems. *CTMC* **2010**, *10* (6), 619–637. <https://doi.org/10.2174/156802610791111506>.
- 510 (28) Pham-The, H.; Cabrera-Pérez, M. Á.; Nam, N.-H.; Castillo-Garit, J. A.; Rasulev, B.; Le-Thi-Thu, H.; Casañola-Martin, G.
511 M. In Silico Assessment of ADME Properties: Advances in Caco-2 Cell Monolayer Permeability Modeling. *CTMC* **2019**,
512 *18* (26), 2209–2229. <https://doi.org/10.2174/1568026619666181130140350>.
- 513 (29) Egan, W. J.; Lauri, G. Prediction of Intestinal Permeability. *Advanced Drug Delivery Reviews* **2002**, *54* (3), 273–289.
514 [https://doi.org/10.1016/S0169-409X\(02\)00004-2](https://doi.org/10.1016/S0169-409X(02)00004-2).
- 515 (30) Vilar, S.; Sobarzo-Sanchez, E.; Santana, L.; Uriarte, E. Ligand and Structure-Based Modeling of Passive Diffusion through
516 the Blood-Brain Barrier. *CMC* **2018**, *25* (9), 1073–1089. <https://doi.org/10.2174/0929867324666171106163742>.
- 517 (31) Barratt, M. D. Quantitative Structure-Activity Relationships for Skin Permeability. *Toxicology in Vitro* **1995**, *9* (1), 27–
518 37. [https://doi.org/10.1016/0887-2333\(94\)00190-6](https://doi.org/10.1016/0887-2333(94)00190-6).
- 519 (32) Wang, N.-N.; Dong, J.; Deng, Y.-H.; Zhu, M.-F.; Wen, M.; Yao, Z.-J.; Lu, A.-P.; Wang, J.-B.; Cao, D.-S. ADME Properties
520 Evaluation in Drug Discovery: Prediction of Caco-2 Cell Permeability Using a Combination of NSGA-II and Boosting. *J.*
521 *Chem. Inf. Model.* **2016**, *56* (4), 763–773. <https://doi.org/10.1021/acs.jcim.5b00642>.
- 522 (33) Fredlund, L.; Winiwarter, S.; Hilgendorf, C. In Vitro Intrinsic Permeability: A Transporter-Independent Measure of Caco-
523 2 Cell Permeability in Drug Design and Development. *Mol. Pharmaceutics* **2017**, *14* (5), 1601–1609.
524 <https://doi.org/10.1021/acs.molpharmaceut.6b01059>.
- 525 (34) Sun, H.; Nguyen, K.; Kerns, E.; Yan, Z.; Yu, K. R.; Shah, P.; Jadhav, A.; Xu, X. Highly Predictive and Interpretable Models
526 for PAMPA Permeability. *Bioorganic & Medicinal Chemistry* **2017**, *25* (3), 1266–1276.
527 <https://doi.org/10.1016/j.bmc.2016.12.049>.
- 528 (35) Gousiadou, C.; Doganis, P.; Sarimveis, H. Development of Artificial Neural Network Models to Predict the PAMPA
529 Effective Permeability of New, Orally Administered Drugs Active against the Coronavirus SARS-CoV-2. *Netw Model Anal*
530 *Health Inform Bioinforma* **2023**, *12* (1), 16. <https://doi.org/10.1007/s13721-023-00410-9>.
- 531 (36) Holton, T. A.; Pollastri, G.; Shields, D. C.; Mooney, C. CPPpred: Prediction of Cell Penetrating Peptides. *Bioinformatics*
532 **2013**, *29* (23), 3094–3096. <https://doi.org/10.1093/bioinformatics/btt518>.
- 533 (37) Williams-Noonan, B. J.; Speer, M. N.; Le, T. C.; Sadek, M. M.; Thompson, P. E.; Norton, R. S.; Yuriev, E.; Barlow, N.;
534 Chalmers, D. K.; Yarovsky, I. Membrane Permeating Macrocycles: Design Guidelines from Machine Learning. *J. Chem.*
535 *Inf. Model.* **2022**, *62* (19), 4605–4619. <https://doi.org/10.1021/acs.jcim.2c00809>.
- 536 (38) Kim, S.; Chen, J.; Cheng, T.; Gindulyte, A.; He, J.; He, S.; Li, Q.; Shoemaker, B. A.; Thiessen, P. A.; Yu, B.; Zaslavsky, L.;
537 Zhang, J.; Bolton, E. E. PubChem 2023 Update. *Nucleic Acids Research* **2023**, *51* (D1), D1373–D1380.
538 <https://doi.org/10.1093/nar/gkac956>.
- 539 (39) Mendez, D.; Gaulton, A.; Bento, A. P.; Chambers, J.; De Veij, M.; Félix, E.; Magariños, M. P.; Mosquera, J. F.; Mutowo,
540 P.; Nowotka, M.; Gordillo-Marañón, M.; Hunter, F.; Junco, L.; Mugumbate, G.; Rodriguez-Lopez, M.; Atkinson, F.; Bosc,
541 N.; Radoux, C. J.; Segura-Cabrera, A.; Hersey, A.; Leach, A. R. ChEMBL: Towards Direct Deposition of Bioassay Data.
542 *Nucleic Acids Research* **2019**, *47* (D1), D930–D940. <https://doi.org/10.1093/nar/gky1075>.
- 543 (40) Juračka, J.; Šrejber, M.; Melíková, M.; Bazgier, V.; Berka, K. MolMeDB: Molecules on Membranes Database. *Database*
544 **2019**, *2019*, baz078. <https://doi.org/10.1093/database/baz078>.

- 545 (41) Berthold, M. R.; Cebron, N.; Dill, F.; Gabriel, T. R.; Kötter, T.; Meinel, T.; Ohl, P.; Thiel, K.; Wiswedel, B. KNIME - the
546 Konstanz Information Miner: Version 2.0 and Beyond. *SIGKDD Explor. Newsl.* **2009**, *11* (1), 26–31.
547 <https://doi.org/10.1145/1656274.1656280>.
- 548 (42) Sugano, K.; Takata, N.; Machida, M.; Saitoh, K.; Terada, K. Prediction of Passive Intestinal Absorption Using Bio-Mimetic
549 Artificial Membrane Permeation Assay and the Paracellular Pathway Model. *International Journal of Pharmaceutics*
550 **2002**, *241* (2), 241–251. [https://doi.org/10.1016/S0378-5173\(02\)00240-5](https://doi.org/10.1016/S0378-5173(02)00240-5).
- 551 (43) Berka, K.; Hendrychová, T.; Anzenbacher, P.; Otyepka, M. Membrane Position of Ibuprofen Agrees with Suggested
552 Access Path Entrance to Cytochrome P450 2C9 Active Site. *J. Phys. Chem. A* **2011**, *115* (41), 11248–11255.
553 <https://doi.org/10.1021/jp204488j>.
- 554 (44) Cramariuc, O.; Rog, T.; Javanainen, M.; Monticelli, L.; Polishchuk, A. V.; Vattulainen, I. Mechanism for Translocation of
555 Fluoroquinolones across Lipid Membranes. *Biochimica et Biophysica Acta (BBA) - Biomembranes* **2012**, *1818* (11),
556 2563–2571. <https://doi.org/10.1016/j.bbamem.2012.05.027>.
- 557 (45) Lundborg, M.; Wennberg, C.; Lindahl, E.; Norlén, L. Simulating the Skin Permeation Process of Ionizable Molecules. *J.*
558 *Chem. Inf. Model.* **2024**, *64* (13), 5295–5302. <https://doi.org/10.1021/acs.jcim.4c00722>.
- 559 (46) R Core Team. R: A Language and Environment for Statistical Computing, 2023. <https://www.R-project.org/>.
- 560 (47) Google. *Welcome to Colaboratory!*
561 <https://colab.research.google.com/gist/lzhou1110/2a30a81cb8c175514ed627bc18016774/hello-colaboratory.ipynb>.
- 562 (48) Goble, C.; Soiland-Reyes, S.; Bacall, F.; Owen, S.; Williams, A.; Eguinoa, I.; Droesbeke, B.; Leo, S.; Pireddu, L.; Rodríguez-
563 Navas, L.; Fernández, J. M.; Capella-Gutiérrez, S.; Ménager, H.; Grüning, B.; Serrano-Solano, B.; Ewels, P.; Coppens, F.
564 Implementing FAIR Digital Objects in the EOSC-Life Workflow Collaboratory. **2021**.
565 <https://doi.org/10.5281/ZENODO.4605654>.
- 566 (49) Lex, A.; Gehlenborg, N.; Strobel, H.; Vuillemot, R.; Pfister, H. UpSet: Visualization of Intersecting Sets. *IEEE Trans.*
567 *Visual. Comput. Graphics* **2014**, *20* (12), 1983–1992. <https://doi.org/10.1109/TVCG.2014.2346248>.
- 568 (50) Barry, P. H.; Diamond, J. M. Effects of Unstirred Layers on Membrane Phenomena. *Physiological Reviews* **1984**, *64* (3),
569 763–872. <https://doi.org/10.1152/physrev.1984.64.3.763>.
- 570 (51) Palumbo, P.; Picchini, U.; Beck, B.; Van Gelder, J.; Delbar, N.; DeGaetano, A. A General Approach to the Apparent
571 Permeability Index. *J Pharmacokinet Pharmacodyn* **2008**, *35* (2), 235–248. <https://doi.org/10.1007/s10928-008-9086-4>.
- 572 (52) Goswami, T.; Li, X.; Jasti, B. R. Effect of Lipophilicity and Drug Ionization on Permeation Across Porcine Sublingual
573 Mucosa. *AAPS PharmSciTech* **2017**, *18* (1), 175–181. <https://doi.org/10.1208/s12249-016-0479-1>.
- 574 (53) Avdeef, A.; Artursson, P.; Neuhoff, S.; Lazorova, L.; Gråsjö, J.; Tavelin, S. Caco-2 Permeability of Weakly Basic Drugs
575 Predicted with the Double-Sink PAMPA Method. *European Journal of Pharmaceutical Sciences* **2005**, *24* (4), 333–349.
576 <https://doi.org/10.1016/j.ejps.2004.11.011>.
- 577 (54) Huque, F. T. T.; Box, K.; Platts, J. A.; Comer, J. Permeability through DOPC/Dodecane Membranes: Measurement and
578 LFER Modelling. *European Journal of Pharmaceutical Sciences* **2004**, *23* (3), 223–232.
579 <https://doi.org/10.1016/j.ejps.2004.07.009>.
- 580 (55) Avdeef, A.; Tsinman, O. PAMPA—A Drug Absorption in Vitro Model. *European Journal of Pharmaceutical Sciences*
581 **2006**, *28* (1–2), 43–50. <https://doi.org/10.1016/j.ejps.2005.12.008>.
- 582 (56) Tsinman, O.; Tsinman, K.; Sun, N.; Avdeef, A. Physicochemical Selectivity of the BBB Microenvironment Governing
583 Passive Diffusion—Matching with a Porcine Brain Lipid Extract Artificial Membrane Permeability Model. *Pharm Res*
584 **2011**, *28* (2), 337–363. <https://doi.org/10.1007/s11095-010-0280-x>.
- 585 (57) Velický, M.; Tam, K. Y.; Dryfe, R. A. W. In Situ Artificial Membrane Permeation Assay under Hydrodynamic Control:
586 Correlation between Drug in Vitro Permeability and Fraction Absorbed in Humans. *European Journal of Pharmaceutical*
587 *Sciences* **2011**, *44* (3), 299–309. <https://doi.org/10.1016/j.ejps.2011.08.007>.
- 588 (58) Colabufo, N. A.; Berardi, F.; Cantore, M.; Perrone, M. G.; Contino, M.; Inglese, C.; Niso, M.; Perrone, R.; Azzariti, A.;
589 Simone, G. M.; Porcelli, L.; Paradiso, A. Small P-Gp Modulating Molecules: SAR Studies on Tetrahydroisoquinoline
590 Derivatives. *Bioorganic & Medicinal Chemistry* **2008**, *16* (1), 362–373. <https://doi.org/10.1016/j.bmc.2007.09.039>.
- 591 (59) Sun, H.; Chow, E. C.; Liu, S.; Du, Y.; Pang, K. S. The Caco-2 Cell Monolayer: Usefulness and Limitations. *Expert Opinion*
592 *on Drug Metabolism & Toxicology* **2008**, *4* (4), 395–411. <https://doi.org/10.1517/17425255.4.4.395>.
- 593 (60) Volpe, D. A. Drug-Permeability and Transporter Assays in Caco-2 and Mdrk Cell Lines. *Future Med. Chem.* **2011**, *3* (16),
594 2063–2077. <https://doi.org/10.4155/fmc.11.149>.
- 595 (61) Zhu, C.; Jiang, L.; Chen, T.-M.; Hwang, K.-K. A Comparative Study of Artificial Membrane Permeability Assay for High
596 Throughput Profiling of Drug Absorption Potential. *European Journal of Medicinal Chemistry* **2002**, *37* (5), 399–407.
597 [https://doi.org/10.1016/S0223-5234\(02\)01360-0](https://doi.org/10.1016/S0223-5234(02)01360-0).
- 598 (62) Von Richter, O.; Glavinas, H.; Krajcsi, P.; Liehner, S.; Siewert, B.; Zech, K. A Novel Screening Strategy to Identify ABCB1
599 Substrates and Inhibitors. *Naunyn-Schmied Arch Pharmacol* **2009**, *379* (1), 11–26. <https://doi.org/10.1007/s00210-008-0345-0>.
- 600 (63) Kerns, E. H.; Di, L.; Petusky, S.; Farris, M.; Ley, R.; Jupp, P. Combined Application of Parallel Artificial Membrane
601 Permeability Assay and Caco-2 Permeability Assays in Drug Discovery. *Journal of Pharmaceutical Sciences* **2004**, *93* (6),
602 1440–1453. <https://doi.org/10.1002/jps.20075>.
- 603 (64) Bittermann, K.; Spycher, S.; Endo, S.; Pohler, L.; Huniar, U.; Goss, K.-U.; Klamt, A. Prediction of Phospholipid–Water
604 Partition Coefficients of Ionic Organic Chemicals Using the Mechanistic Model COSMO Mic. *J. Phys. Chem. B* **2014**, *118*
605 (51), 14833–14842. <https://doi.org/10.1021/jp509348a>.
- 606
607

- 608 (65) Stenberg, P.; Norinder, U.; Luthman, K.; Artursson, P. Experimental and Computational Screening Models for the
609 Prediction of Intestinal Drug Absorption. *J. Med. Chem.* **2001**, *44* (12), 1927–1937.
610 <https://doi.org/10.1021/jm001101a>.
- 611 (66) Teksin, Z. S.; Seo, P. R.; Polli, J. E. Comparison of Drug Permeabilities and BCS Classification: Three Lipid-Component
612 PAMPA System Method versus Caco-2 Monolayers. *AAPS J* **2010**, *12* (2), 238–241. [https://doi.org/10.1208/s12248-](https://doi.org/10.1208/s12248-010-9176-2)
613 [010-9176-2](https://doi.org/10.1208/s12248-010-9176-2).
- 614 (67) Fujikawa, M.; Nakao, K.; Shimizu, R.; Akamatsu, M. QSAR Study on Permeability of Hydrophobic Compounds with
615 Artificial Membranes. *Bioorganic & Medicinal Chemistry* **2007**, *15* (11), 3756–3767.
616 <https://doi.org/10.1016/j.bmc.2007.03.040>.
- 617 (68) Avdeef, A.; Nielsen, P. E.; Tsinman, O. PAMPA—a Drug Absorption in Vitro Model: 11. Matching the in Vivo Unstirred
618 Water Layer Thickness by Individual-Well Stirring in Microtitre Plates. *European Journal of Pharmaceutical Sciences*
619 **2004**, *22* (5), 365–374. <https://doi.org/10.1016/j.ejps.2004.04.009>.
- 620 (69) Brunner, J.; Graham, D. E.; Hauser, H.; Semenza, G. Ion and Sugar Permeabilities of Lecithin Bilayers: Comparison of
621 Curved and Planar Bilayers. *J. Membr. Biol.* **1980**, *57* (2), 133–141. <https://doi.org/10.1007/BF01868999>.
- 622 (70) Helander, H. F.; Fändriks, L. Surface Area of the Digestive Tract – Revisited. *Scandinavian Journal of Gastroenterology*
623 **2014**, *49* (6), 681–689. <https://doi.org/10.3109/00365521.2014.898326>.
- 624 (71) Schiller, C.; Frohlich, C.-P.; Giessmann, T.; Siegmund, W.; Monnikes, H.; Hosten, N.; Weitschies, W. Intestinal Fluid
625 Volumes and Transit of Dosage Forms as Assessed by Magnetic Resonance Imaging. *Aliment Pharmacol Ther* **2005**, *22*
626 (10), 971–979. <https://doi.org/10.1111/j.1365-2036.2005.02683.x>.
- 627 (72) Hubatsch, I.; Ragnarsson, E. G. E.; Artursson, P. Determination of Drug Permeability and Prediction of Drug Absorption
628 in Caco-2 Monolayers. *Nat Protoc* **2007**, *2* (9), 2111–2119. <https://doi.org/10.1038/nprot.2007.303>.
- 629 (73) Deur, C.; Agrawal, A. K.; Baum, H.; Booth, J.; Bove, S.; Brieland, J.; Bunker, A.; Connolly, C.; Cornicelli, J.; Dumin, J.;
630 Finzel, B.; Gan, X.; Guppy, S.; Kamilar, G.; Kilgore, K.; Lee, P.; Loi, C.-M.; Lou, Z.; Morris, M.; Philippe, L.; Przybranowski,
631 S.; Riley, F.; Samas, B.; Sanchez, B.; Teclé, H.; Wang, Z.; Welch, K.; Wilson, M.; Yates, K. N-(6,7-Dichloro-2,3-Dioxo-
632 1,2,3,4-Tetrahydroquinoxalin-5-Yl)-N-Alkylsulfonamides as Peripherally Restricted N-Methyl-D-Aspartate Receptor
633 Antagonists for the Treatment of Pain. *Bioorganic & Medicinal Chemistry Letters* **2007**, *17* (16), 4599–4603.
634 <https://doi.org/10.1016/j.bmcl.2007.05.083>.
- 635 (74) Chiba, J.; Iimura, S.; Yoneda, Y.; Watanabe, T.; Muro, F.; Tsubokawa, M.; Iigou, Y.; Satoh, A.; Takayama, G.; Yokoyama,
636 M.; Takashi, T.; Nakayama, A.; Machinaga, N. Synthesis and Biological Evaluation of Benzoic Acid Derivatives as Potent,
637 Orally Active VLA-4 Antagonists. *Bioorganic & Medicinal Chemistry* **2007**, *15* (4), 1679–1693.
638 <https://doi.org/10.1016/j.bmc.2006.12.006>.
- 639 (75) Flaten, G. E.; Kottra, G.; Stensen, W.; Isaksen, G.; Karstad, R.; Svendsen, J. S.; Daniel, H.; Svenson, J. In Vitro
640 Characterization of Human Peptide Transporter hPEPT1 Interactions and Passive Permeation Studies of Short Cationic
641 Antimicrobial Peptides. *J. Med. Chem.* **2011**, *54* (7), 2422–2432. <https://doi.org/10.1021/jm1015704>.
- 642 (76) Holz, M.; Heil, S. R.; Sacco, A. Temperature-Dependent Self-Diffusion Coefficients of Water and Six Selected Molecular
643 Liquids for Calibration in Accurate 1H NMR PFG Measurements. *Phys. Chem. Chem. Phys.* **2000**, *2* (20), 4740–4742.
644 <https://doi.org/10.1039/b005319h>.
- 645 (77) Derrick, T. S.; McCord, E. F.; Larive, C. K. Analysis of Protein/Ligand Interactions with NMR Diffusion Measurements:
646 The Importance of Eliminating the Protein Background. *Journal of Magnetic Resonance* **2002**, *155* (2), 217–225.
647 <https://doi.org/10.1006/jmre.2002.2513>.
- 648 (78) Amidon, G. L.; Lennernäs, H.; Shah, V. P.; Crison, J. R. A Theoretical Basis for a Biopharmaceutical Drug Classification:
649 The Correlation of in Vitro Drug Product Dissolution and in Vivo Bioavailability. *Pharmaceutical Research* **1995**, *12* (3),
650 413–420. <https://doi.org/10.1023/A:1016212804288>.
- 651